

# Detection of Thermal Donors from Electrically Active Oxygen Interstitials by Optical Second Harmonic Generation

Ming Lei, Jacqueline Zou, Justin Lee, John Changala and Brian Larzelere

Femtometrix Inc

Irvine, USA

Ming.Lei@femtometrix.com

**Abstract** –Substrate resistivity stability has become the most critical control for radio frequency (RF) device manufacturing. In this paper, we demonstrate nonlinear optics based metrology to measure electrically active oxygen interstitial sites (Oi) in high resistive bulk Si wafers, which are vulnerable to electric and mechanical property drift during device fabrication. Time dependent second harmonic generation (TD-SHG) governed by electric-field induced second harmonic (EFISH) effect provides consistent detection of thermal donors originating from Oi distributed near Si interface. The successful concept proof can be extended to test pad design for in-line monitor of substrate resistivity variations from annealing processes.

## I. INTRODUCTION

Manufacturing of radio frequency (RF) devices operating in GHz and THz frequency range is facing great integration challenges with proper substrates. High resistive (HR) substrate is beneficial to RF device performance and power efficiency by reducing insertion loss and parasitic cross-talks while improving quality factor and linear characteristics of passive components. However, control of interstitial oxygen (Oi) to balance between high resistivity and mechanical hardness becomes the largest bottleneck for integration of HR silicon platform. Oxygen interstitials ([Oi]), as one of the most common intrinsic impurities during single crystal silicon growth by the Czochralski (CZ) process [1], are essential for yield since they can serve as precipitate centers to getter metallic contaminants and split lines and keep them away from active device area. On the other hand, residual interstitial oxygens can form thermal donors upon annealing at temperature in the range of 300~500°C, which alter the effective doping concentration and device characteristics. Especially for p-type substrate, this may flip the doping polarity depending on the background dopant level. Thus, monitor of [Oi] in HR silicon wafer becomes critical for process control and yield improvement of RF device manufacturing. In addition to destructive characterizations by mass spectrometry and other elemental analysis, the conventional metrology for interstitial oxygen content in HR Si wafers is Fourier transform infrared (FTIR) spectroscopy.

FTIR detects the absorption line centered at 1107 cm<sup>-1</sup> associated with the stretching mode of Si-O-Si bonds at room temperature [2]. In order to obtain good signal-to-noise ratio, minimum sample thickness 1~3 mm is usually required. Therefore, a thick chunk from the same Si ingot is sampled to estimate the oxygen content for the entire wafer batch. To control [Oi] on wafer level from wafer start to process cycles during device manufacturing, noninvasive and in-line monitor methodology becomes an urgent need for both wafer vendors and fabs.

Continuous downscaling of transistor size with more integrated chip functions has been the main driving power of semiconductor industry. However, Moore's law driven roadmap encountered fundamental limit for traditional geometric scaling. Novel materials and architectures were introduced in advanced technology manufacturing driven by mobile market growth, which have extended scaling in another dimension, but also posed great challenges to process control and yield management. Optical second harmonic generation (SHG) is a versatile and non-invasive technique that can address the requirement for advanced technology manufacturing. SHG stems from the higher order nonlinearity in the optical response from interface or bulk region of semiconductor materials, which leads to unique information of atomic scale disorder related to interfacial and crystalline properties [3-7]. In this paper, we will introduce the basic physics of optical SHG in characterizing critical interfacial electric properties, and evaluate its application in detection of electrically active [Oi] and capabilities beyond.

## II. FUNDAMENTALS OF SECOND HARMONIC GENERATION

### A. Electric-Field Induced Second Harmonic Effect

Optical response at visible to near infrared spectral range comes from oscillation of bound electrons excited by external optical field, which is well known as the Lorentz model [8]. Under low field linear restoring force approximation, electrons will absorb the incident photon and reemit another photon at the same frequency/energy, which give rise to abundant linear

optical phenomena. Furthermore, under high optical field regime from pulsed laser illumination, departure from linear oscillation of electrons can result in optical radiation at doubled frequency  $2\omega$  or energy ( $E = 2 \square\omega$ ), irradiated by fundamental frequency  $\omega$  [8]. Specifically, for the case of centrosymmetric semiconductors, the lowest order dipolar contribution from bulk crystal is forbidden, except for the interface region where inversion symmetry is broken due to medium discontinuity [8]. This results in relatively strong dipole response from the interface region which is dominating in total SHG, and weak bulk signal through quadrupolar or higher order process. This unique property enables the exclusive sensitivity of SHG specific to interfacial electric properties, such as charge traps, band offsets, doping level, etc. Upon the presence of interfacial electric field, the inversion symmetry of the intrinsic lattice within the space charge region (SCR) is broken. As a result, a non-vanishing bulk dipolar radiation arises from the spatial extent of SCR, which is known as electric-field induced second harmonic (EFISH) generation [9]. The intensity of SHG radiation  $I^{(2\omega)}$  can be expressed as:

$$I^{(2\omega)}(t) \propto \left| \chi_{\text{eff}}^{(2)} + \int_0^{W_{\text{SCR}}} \chi_{\text{eff}}^{(3)} E_{DC}(t, z) e^{ik_z z} dz \right|^2 (E^{(\omega)})^2 \quad (1),$$

where  $\chi_{\text{eff}}^{(2)}$  is the equilibrium 2<sup>nd</sup> order nonlinear susceptibility,  $\chi_{\text{eff}}^{(3)}$  represents the 3<sup>rd</sup> order nonlinear susceptibility to couple interfacial electric field  $E_{DC}$  and optical field  $E^{(\omega)}$  within SCR. For SHG radiation in near UV spectral range, the penetration depth in most semiconductor materials (Si for example) is usually much smaller than the SCR width  $W_{\text{SCR}}$ . Accordingly, EFISH signal can be simplified as:

$$I^{(2\omega)}(t) \propto \left| \chi_{\text{eff}}^{(2)} + \chi_{\text{eff}}^{(3)} E_{DC}^0(t) \right|^2 \quad (2),$$

where  $E_{DC}^0$  is the electric field at interface.

### B. Time Dependent SHG

Eq. (2) describes how the built-in electric field at semiconductor interface modulates SHG, which renders the interface specific sensitivity. For a typical semiconductor/oxide interface structure, upon illumination by pulsed laser, photocarriers (electrons and holes) are generated within the semiconductor substrate absorption depth. Carriers that gain enough energy through multi-photon absorption process can overcome the energy barrier determined by the band offsets between semiconductor and oxide. When the oxide layer is thin enough (compared to the mean free path of carriers within oxide), photocarriers can be injected to occupy the surface trap sites as depicted in Fig. 1. For most semiconductor materials, the conduction band (CB) offset is usually smaller than the valence band (VB) offset. Therefore, the hole injection probability is much smaller due to the larger energy barrier height ( $\varphi_h > \varphi_e$ ), and electron injection is generally dominant in this internal multiphoton photoemission (IMPE) process. With electrons trapped on surface sites, positively charged holes are left in substrate. This space charge distribution leads to the

formation of built-in electric field  $E_{DC}(t, z)$ . The time dependence originates from cumulative charge injection and trapping upon continuous laser irradiation until this built-in electric field can counterbalance the forward charge injection process.

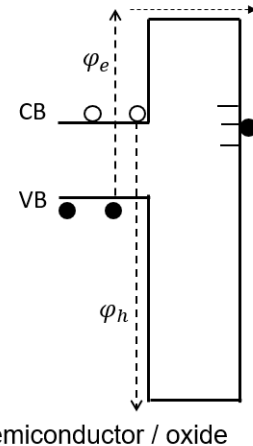


Fig. 1. Band diagram of typical semiconductor/oxide interface under illumination by pulsed laser. Filled circles: photo-generated electrons; empty circles: holes.

Hence the corresponding time dependent (TD)-SHG signal offers good measure for the characteristics of interfacial electric properties related to charging kinetics. As a first order approximation for a single charge injection process, the net trapped charges  $n(t)$  can be described by the following rate equation:

$$\frac{dn(t)}{t} = \frac{N - n(t)}{\tau_1} - \frac{n(t)}{\tau_2} \quad (3),$$

where  $N$  is the nominal total available trap states,  $\tau_1$  is the corresponding trapping constant,  $\tau_2$  the detrapping constant. With special initial condition (at  $t = 0$ , interfacial charges as well as electric field remain neutral):  $n(0) = 0$ , the formal solution of Eq. (3) yields trapped charge density as a function of laser exposure time:

$$n(t) = n_0 (1 - e^{-t/\tau}) \quad (4),$$

where  $1/\tau = 1/\tau_1 + 1/\tau_2$ ,  $n_0 = N\tau_2/(\tau_1 + \tau_2)$ . The corresponding electric field at interface varies in the same way as trapped charges  $E_{DC}(t) = n(t)/\epsilon$ , which leads to the time dependent SHG signal described in Eq. (2). Note that if multiple charge injection/trapping mechanisms occur at the same time, the explicit solution of  $n(t)$  will be more complicated with more than one exponential component representing each charging kinetics.

### III. OXYGEN INTERSTITIALS AND THE IMPACT TO TD-SHG

P-type samples with two types of [O<sub>i</sub>] within the process window have been selected for testing by SHG as listed in Table I. Nominal [O<sub>i</sub>] were determined by FTIR spectroscopy from the same ingot batch with low (2 ppma: part per million atoms) and high (6 ppma) oxygen concentrations. And one wafer from each group was sent to thermal anneal at ~400 °C for 30 mins at N<sub>2</sub> environment which has been used as a

standard annealing condition during RF device fabrication. Interstitial oxygens in CZ Si crystals usually exist in the form of O-Si-O complex. Upon low temperature anneal at 300~600 °C, shallow states near the CB edge are created at Oi sites, which are converted into electrically active thermal donors [1, 2].

TABLE I. SAMPLE DESCRIPTION

	No Anneal	Anneal
Low [O <sub>i</sub> ] (2 ppma)	A <sub>0</sub>	A <sub>1</sub>
High [O <sub>i</sub> ] (6 ppma)	B <sub>0</sub>	B <sub>1</sub>

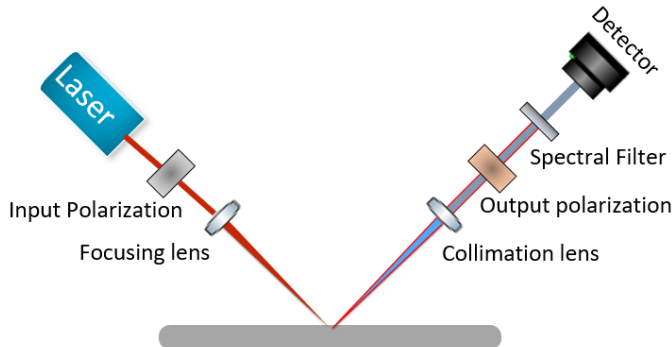


Fig. 2. Schematic layout of optical setup for SHG signal detection.

P-polarized SHG signal (spectroscopically centered at 390 nm) was collected from wafers under excitation by p-polarized fundamental radiation (780 nm), as described by the optical setup in Fig. 2. Fundamental laser pulses were focused at 45° incident angle to a ~50 μm diameter spot on the wafer surface. Full wafer scans with uniform sampling of total 293 grid points at 10 mm spacing were collected for all wafers. From the rotational anisotropy (RA)-SHG data in Fig. 3, a typical 4-fold symmetry pattern stemming from Si(100) crystal plane [10] is demonstrated from all wafers. Thus, wafer orientation with 0° azimuthal angle (notch down) was selected for all wafers.

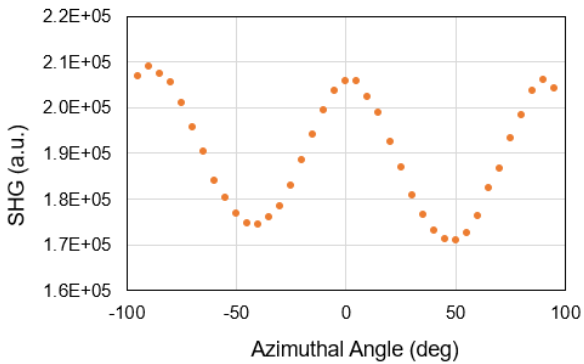


Fig. 3. RA-SHG from wafer B<sub>1</sub>. 0° azimuthal angle corresponds to notch down orientation.

There are some important observations from the TD-SHG results as shown in Fig. 4. Two groups of time dependent behaviors are clearly present, according to annealing process. Group 1 samples (A<sub>1</sub>, B<sub>1</sub>) exhibit much higher (~30% more) initial SHG signal ( $I_0$ ) than Group 0 (A<sub>0</sub>, B<sub>0</sub>). Within group 1,

B<sub>1</sub> also shows overall higher signal compared to A<sub>1</sub>. Although Group 0 samples start with lower  $I_0$ , the initial signal decline at the initial 0.25s is followed by a fast increase which leads to eventually surpassing the SHG signals from Group 1 samples after 4s. In Practice, much shorter scan time can be used for balanced sensitivity and throughput. The large time range displayed here is only used to exploit the origin of charge kinetics.

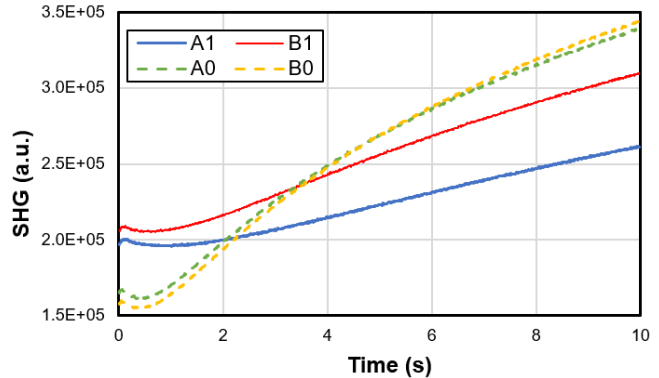


Fig. 4. TD-SHG signal from test samples listed in Table I. The curves are averaged over ~300 points uniformly sampled from each wafer by 10mm spacing.

The difference in TD-SHG kinetics is mostly determined by the effective dopant concentration which has strong correlation with annealing process related to electrically active [O<sub>i</sub>].

For Group 0 samples (A<sub>0</sub>, B<sub>0</sub>), despite the difference in oxygen content from the as-grown Si wafers, identical TD behaviors from the same P-type substrate doping are expected since [O<sub>i</sub>] remain inactive and have no impact to TD-SHG. Hence, the corresponding EFISH effect affected by charging kinetics leads to TD response from a typical P-type substrate: initial decline followed by increase of SHG signal. This inverted response reflects the charging change of interface states and SCR during IMPE process.

For Si crystal exposed in air, a thin native oxide layer is usually formed at equilibrium. With poor Si/SiO<sub>x</sub> interface quality from native oxide, high interface trap density (D<sub>it</sub>) is created. Usually, “donor” like interface states exist below the neutral level, which leads to positively charged interface states [11]. Consequently, negative charges from ionized acceptors and thus depletion states are induced in SCR as presented in Fig. 5(a). Upon laser irradiation, electrons are injected to occupy surface trap states, and Si band bending is changed to accumulation with holes left in substrate. The surface charging states and band bending are depicted in Fig. 5. As a result, the inverted time dependent response from Group 0 samples is because of the change in band bending states as well as the corresponding electric field  $E(t)$ . Also note that positive charges at interface states (D<sub>it</sub>) continue to increase when the band is bent upwards.

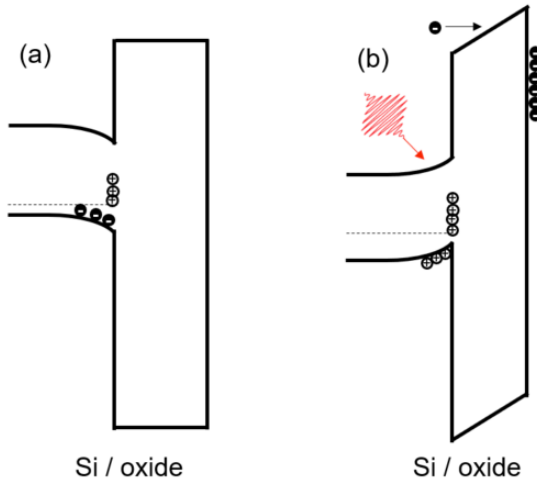


Fig. 5. Band diagram of P-type Si/oxide interface without (a) and with (b) pulsed laser illumination.

For Group 1 wafers subject to thermal anneal, compensation doping from electrically active [O<sub>i</sub>] has flipped the effective substrate doping to N-type. At equilibrium, negative charges from “acceptor” like interface states induce depletion within SCR. Laser induced electron injection doesn’t change the charge polarity of SCR or band bending direction, which makes TD-SHG signal dominant by increase. With higher [O<sub>i</sub>] or thermal donors, larger band bending leads to larger electric field  $E(t)$  as well as TD-SHG signal  $I^{(2\omega)}(t)$  from the EFISH effect described by Eq. (2). This explains the difference in TD-SHG signal within Group 1 samples, where B<sub>1</sub> has overall higher thermal donor concentration than A<sub>1</sub>. Furthermore, comparing the band diagrams in Fig. 5(b) and Fig. 6(b), additional contribution from interfacial trapped charges can lead to larger electric field strength at accumulation. After large enough amounts of electrons are injected, the electric field strength at interface from Group 0 samples may exceed that from Group 1.

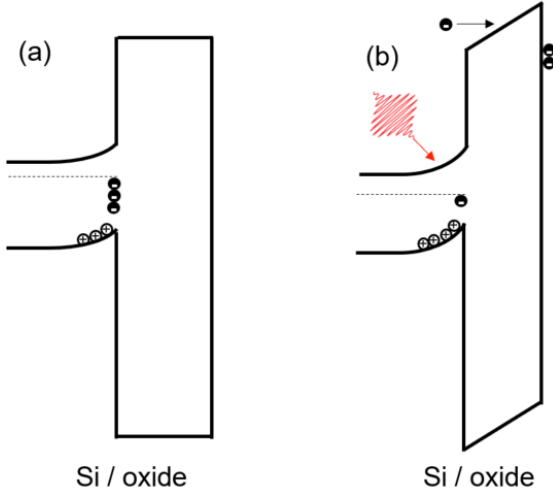


Fig. 6. Band diagram of N-type Si/oxide interface without (a) and with (b) pulsed laser illumination.

In conclusion, TD-SHG signal from annealed wafers (A<sub>1</sub>, B<sub>1</sub>) is determined by thermal donors. Therefore, SHG wafer

maps indicate the corresponding lateral spatial distribution of thermal donors which are proportional to [O<sub>i</sub>]. As displayed in Fig. 7, TD-SHG signal increases towards the wafer edge region. This radial dependence of [O<sub>i</sub>] may originate from the temperature gradient, and consequently non-uniform incorporation of oxygen content during crystal growth.

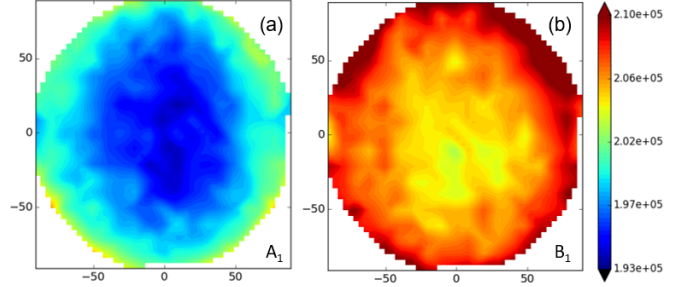


Fig. 7. SHG wafer maps from sample A<sub>1</sub> (a) and B<sub>1</sub> (b). The SHG signal value is averaged over the initial 0.5s.

Based on EFISH effect, SHG signal is not responding to electrically inactive [O<sub>i</sub>], which makes it not possible to detect atomic state of oxygen content in as-cut wafers. In addition, limited by the linear absorption of SHG radiation in Si, only the region ~30nm below interface can be directly detected. Therefore, SHG provides selective detection of electrically active [O<sub>i</sub>] near the active device region. However, this makes it quite suitable for in-line process monitor during semiconductor device high volume manufacturing, especially with test pad incorporated into product wafer design.

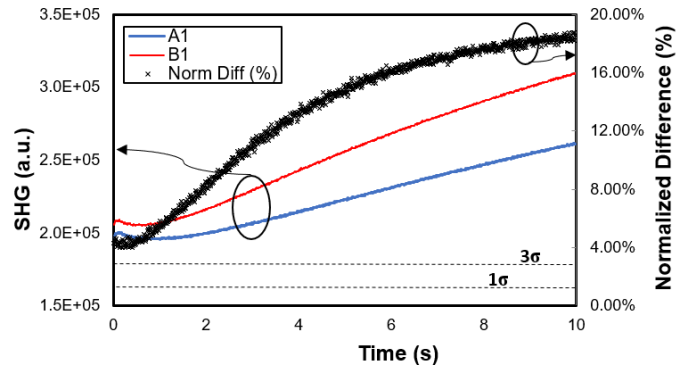


Fig. 8. Normalized difference between sample A<sub>1</sub> and B<sub>1</sub> for the corresponding time dependent response. 1 $\sigma$  and 3 $\sigma$  detection limits are from repeatability measurement.

In order to determine the detectability of [O<sub>i</sub>] distinction, repeatability measurement of SHG signal from 15 repeatable scans shows standard deviation with typical value of 1%. This indicates that for any signal difference larger than ~3%, we would expect consistent detection with good confidence (99.7% for normal distribution). However, if the signal difference is too small, trade off between sensitivity and throughput may have to be made by extending the scan time. As indicated in Fig. 8, the normalized difference ( $|I_{B1}^{(2\omega)} - I_{A1}^{(2\omega)}| / I_{A1}^{(2\omega)}$ ) would increase with time, thus longer scan time may lead to better detectability in general. Since the signal difference for sample A<sub>1</sub> and B<sub>1</sub> is well above 3 $\sigma$  limit, short exposure time (<1s) at the initial portion of TD curves in

Fig. 5 is more than enough for good detection of [Oi] difference.

So far, only qualitative results consistent with FTIR have been demonstrated by TD-SHG. More quantitative modeling and correlation study with other metrologies, such as secondary ion mass spectrometry (SIMS) will be conducted in the future.

#### IV. SUMMARY

In this paper we discussed the fundamental physics of EFISH effect and its application in detection of thermal donors in HR Si wafers. The non-contact nature of this nonlinear optical metrology with fast scan speed provides selective detection as well as spatial distribution of thermal donors. Moreover, the same operation principles can be applied to other types of electric defects, such as  $D_{it}$ [3], oxide charge [5], interfacial dipole layers, which renders SHG the only charge sensitive optical metrology.

#### ACKNOWLEDGMENT

We would like to thank Victer Chan, David Kim and Dornisch Dieter from Jazz Semiconductor for their great help on providing test samples and discussion about scan results.

#### REFERENCES

- [1] R. C. Newman, "Oxygen diffusion and precipitation in Czochralski silicon," *J. Phys. Condens. Matter*, vol. 12, pp. R335–R365, January 2000.
- [2] R. Stoudek, J. Humlincek, "Infrared spectroscopy of oxygen interstitials and precipitates in nitrogen-doped silicon," *Physica B*, vol. 376-377, pp. 150-153, April 2006.
- [3] T. Scheidt, E. G. Rohwer, P. Neethling, H. M. von Bergmann, and H. Stafast, "Ionization and shielding of interface states in native p<sup>+</sup>-Si/SiO<sub>2</sub> probed by electric field induced second harmonic generation," *J. Appl. Phys.*, vol. 104, pp. 083712, 2008.
- [4] J. Price, Ming Lei, P. S. Lysaght, G. Bersuker, and M. C. Downer, "Charge trapping defects in Si/SiO<sub>2</sub>/Hf<sub>(1-x)</sub>Si<sub>x</sub>O<sub>2</sub> film stacks characterized by spectroscopic second-harmonic generation," *J. Vac. Sci. Technol. B*, vol. 29, pp. 04D101, 2011.
- [5] J. J. H. Gielis, B. Hoex, M. C. M. van de Sanden, and W. M. M. Kessels, "Negative charge and charging dynamics in Al<sub>2</sub>O<sub>3</sub> films on Si characterized by second-harmonic generation," *J. Appl. Phys.*, vol. 104, pp. 073701, 2008.
- [6] Ming Lei, J. Price and M. C. Downer, "Hot carrier injection from nanometer-thick silicon-on-insulator films measured by optical second-harmonic generation," *Appl. Phys. Lett.*, vol. 96, pp. 241105, 2010.
- [7] Ming Lei, J. Price, Wei-E Wang, Man Hoi Wong, Ravi Droopad, Paul Kirsch, G. Bersuker, and M. C. Downer, "Characterization of anti-phase boundaries in heteroepitaxial polar-on-nonpolar semiconductor films by optical second-harmonic generation," *Appl. Phys. Lett.*, vol. 102, pp. 152103, 2013.
- [8] R. Boyd, "Nonlinear Optics," 3rd edition, Academic Press, Burlington, MA, 2008.
- [9] O. A. Aktsipetrov, A. A. Fedyanin, A. V. Melnikov, E. D. Mishina, A. N. Rubtsov, M. H. Anderson, P. T. Wilson, M. ter Beek, X. F. Hu, J. I. Dadap, and M. C. Downer, "dc-electric-field-induced and low-frequency electromodulation second-harmonic generation spectroscopy of Si(001)-SiO<sub>2</sub> interfaces," *Phys. Rev. B*, vol. 60, pp. 8924, September 1999.
- [10] J. E. Sipe, D. J. Moss, and H. M. van Driel, "Phenomenological theory of optical second- and third-harmonic generation from cubic centrosymmetric crystals," *Appl. Phys. Lett.*, vol. 35, pp. 1129, January 1987.
- [11] S. M. Sze and Kwok K. Ng, "Physics of Semiconductor Devices," 3<sup>rd</sup> edition, Wiley-Interscience, New York, 2006.